Mixed Spin-1 and Spin-3/2 BC Ferromagnetic System On the Two-fold Cayley Tree

Rachidi A. Yessoufou[1,2,3], Victor A. Kpadonou[2] and Felix Hontinfinde[2,3]
[2] *Département de Physique (FAST) et Institut de Mathématiques et de Sciences Physiques (IMSP), University of Abomey-Calavi, Porto-Novo, Republic of Benin*
[3] *The Abdus Salam International Centre for Theoretical Physics (ICTP), Trieste, Italy*

The mixed spin-1 and spin-3/2 BC Ising ferromagnetic system is studied on the two-fold Cayley tree by means of the exact recursion relations. The exact expressions for the magnetization, the quadripolar moment, the Curie temperature, and the free energy are found, and the phase diagrams are constructed on the Cayley tree with the coordination numbers $q = 3, 4$ and 6 for various values of the single-ion anisotropy constants $\Delta_1 = D1/J$ for spin-1 and $\Delta_2 = D2/J$ for spin-3/2. The existence of tricritical point is investigated for different values of the coordination numbers q and the single-ion anisotropy values. Phase diagrams in the plan $(kT/J, \Delta_1)$ are constructed when first $\Delta_1 = \Delta_2$ and second $\Delta_1 \neq \Delta_2$ for selected values of Δ_2. The thermal dependence of the magnetization is also studied. The results found are compared with those of other approximate methods.

1. Introduction

Mixed Ising spin systems have attracted much interest over the past few years from both theoretical and experimental points of view. This is due to their relevance in studying molecular-based magnetic materials which exhibit ferromagnetic properties [1] and also to their technological applications in the domain of thermomagnetic recording [2]. Mixed Ising spin models appear simpler in the description of a system that shows the tricritical point (TCP) behaviour. Moreover, they are useful to study the effect of inhomogeneities on the phase diagram of Ising systems. When defined on hierarchical graphs, such as the Bethe lattice or the Cayley tree, interesting statistical properties are expected. The properties of such Ising systems have been studied by well-known methods of equilibrium statistical mechanics. One of the earliest, simplest and the most extensively studied mixed-spin Ising model is the spin-1/2 and spin-1 mixed system. This system has been studied using the renormalization-group technique [3], high-temperature series expansions [4], the free-fermion approximation [5], the recursion method [6], the Bethe-Peierls approximation [7], the framework of the effective-field theory [8, 9], the mean-field approximation [10, 11], the finite cluster approximation [12], the Monte-Carlo simulation [13, 14], the mean-field renormalization-group technique [15], a numerical transfert matrix study [16] and the cluster method in pair-approximation [17]. Even though most of these studies have focused on the mixed spin-1/2 and spin-s ($s > 1/2$) Ising systems, the mixed-spin Ising systems consisting of higher spins are not without interest. Indeed, several theoretical studies of the two-sublattices mixed spin-1 and spin-3/2 Ising models have been reported based on the effective-field theory with correlations that correctly incorporate the single-site kinematic relations of the spin operators on a honeycomb lattice [18], on a square lattice [19], on the simple cubic lattice [20], within the mean-field theory based on the Bogoliubov inequality for Gibbs free energy [21], and by the means of recursion relations on the Bethe lattice [22, 23]. Albayrak studied the mixed spin-1 and spin-3/2 on the Bethe lattice using the exact recursion equations and found a tricritical point for some values of the coordination number q [22]. The presence of lattice anisotropy in the model is interesting since it might induce a profound influence on the molecular magnetism of this system. More recently, Cesur Ekiz [23] used the same technique to investigate the same model of mixed spin on the Bethe lattice in the ferromagnetic case and obtained interesting results like the existence of compensation temperatures, which have great technological importance.

The aim of this paper is to present an exact formulation of the mixed spin-1 and spin-3/2 Ising ferromagnetic system as a non-linear discrete two-dimensional mapping on the two-fold Cayley tree

[1] yesradca@yahoo.fr

using the recursion relations, to obtain the phase diagrams for various values of single ion-anisotropy constants or crystal field interaction Δ_1 for the spin-1 and Δ_2 for the spin-3/2, and to clarify the effects of the crystal field interaction on the magnetic properties of the system. The existence of tricritical points are investigated depending on the values of the single-ion anisotropy constants and the coordination numbers. The exact expressions for the magnetization, the quadripolar moment parameter, the free energy and the second-order phase transition temperature are obtained in terms of the recursion relations. The obtained phase diagrams are compared with the results of the above mentioned references for spin-1 and spin-3/2 Ising systems.

The outline of this work is as follows. In Section 2, the formulation of the problem is given and the exact expressions for dipole and quadripolar moment parameters are obtained. The exact expressions for the Curie or the second-order transition temperature and the free energy are obtained and the phase diagrams are presented in Section 3. In Section 4 a summary and dicussion of the phase diagrams are given.

2. The Formulation of the Problem

2.1. Definition of the model

The two-fold Cayley tree is constructed as follows. First, we considered two points O and O' as the central points of the graph (see Fig.1) [24]. The "first shell" of the graph is obtained by constructing q points that connect to each central point. For the central point O, one gets the "first left shell" whereas for O', one obtains the first opposite shell named "the first right shell". The graph grows further from these q points by connection to $(q-1)$ new points and so on. At the end, one has a two-fold Cayley tree with a frontier shell (absent in the Bethe lattice) that has closed loops. The two-fold Cayley tree consists of two sublattices A and B.

Discrete spin values are put on the Cayley tree with spin-1 on the sublattice A (variable s) and spin-3/2 on sublattice B (variable σ). Then, $s_i = \pm 1, 0$ and $\sigma_j = \pm 3/2, \pm 1/2$ are the possible spin variables on sites of the two sublattices.

The interaction hamiltonian of this mixed spin system is defined as:

$$H = -J\sum_{i,j} s_i\sigma_j - D_1\sum_i s_i^2 - D_2\sum_j \sigma_j^2 \qquad (1)$$

Where, $J > 0$ is the ferromagnetic nearest-

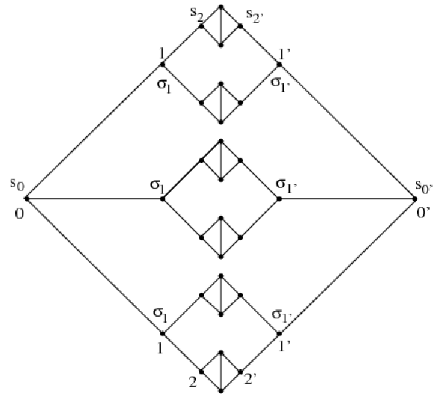

Figure 1: A two-fold Cayley tree for coordination $q = 3$ consisting of two different types of magnetic atoms A and B with spin variables s_i and σ_j , respectively.

neighbour exchange coupling constant, D_1 and D_2 are the crystal-field or lattice anisotropy for spin-1 and spin-3/2, respectively. In this equation, the first sum runs over nearest-neighbour spin pairs, the second over sites of the sublattice A and the third over sites of the second sublattice B.

The partition function of this mixed spin system is given by:

$$\begin{aligned} Z &= \sum_{i,j} e^{-\beta H} \\ &= \sum_{i,j} e^{-\beta(-J\sum_{i,j} s_i\sigma_j - D_1\sum_i s_i^2 - D_2\sum_i \sigma_i^2)} \end{aligned} \qquad (2)$$

where, $\beta = 1/kT$, with k the Boltzmann constant and T the temperature. The magnetizations are computed from some exact recursion relations that we treated by means of an iteration procedure. In fact, the graph splits into q disconnected pieces when cut at the central points O and O'. Therefore, the partition function can be written as follows:

$$Z = \sum_{s_0}\sum_{s_{0'}} e^{-\beta D_1(s_0^2 + s_{0'}^2)} g_n^q(s_0, s_{0'}) \qquad (3)$$

where s_0 and $s_{0'}$ are the central spin values and $g_n(s_0, s_{0'})$ denotes the partition of an individual branch. Its explicit expression is:

$$\begin{aligned} & g_n(s_0, s_{0'}) = \\ & \sum_{\sigma_1}\sum_{\sigma_{1'}} \exp[\beta(Js_0\sigma_1 + Js_{0'}\sigma_{1'} - D_2(\sigma_1^2 + \sigma_{1'}^2) \\ & \qquad + J\sum_{i,j} s_i\sigma_j + D_1\sum_i s_i^2 + D_2\sum_j \sigma_j^2)] \end{aligned} \qquad (4)$$

Each branch can be cut on the sites σ_1 or $\sigma_{1'}$, which are the nearest-neighbour to the central point, respectively. Thus, one gets the following recurrence relations for $g_n(s_0, s_{0'})$ and $g_{n-1}(\sigma_1, \sigma_{1'})$:

$$g_n(s_0, s_{0'}) = \sum_{\sigma_1}\sum_{\sigma_{1'}} \exp[\beta(Js_0\sigma_1 + Js_{0'}\sigma_{1'} - D_2(\sigma_1^2 + \sigma_{1'}^2))]g_{n-1}^{q-1}(\sigma_1, \sigma_{1'}) \quad (5)$$

and

$$g_{n-1}(\sigma_1, \sigma_{1'}) = \sum_{s_2}\sum_{s_{2'}} \exp[\beta(Js_2\sigma_1 + Js_{2'}\sigma_{1'} - D_1(s_2^2 + s_{2'}^2))]g_{n-2}^{q-1}(s_2, s_{2'}) \quad (6)$$

Thus, for $g_n(1,1)$ and $g_{n-1}(\frac{3}{2},\frac{3}{2})$ as examples, the explicit expressions read:

$$\begin{aligned} g_{n-1}(\frac{3}{2},\frac{3}{2}) &= e^{\beta(3J+2D_1)}g_{n-2}^{q-1}(1,1) \\ &+2e^{\beta(\frac{3J}{2}+D_1)}g_{n-2}^{q-1}(1,0) \\ &+2e^{(2\beta D_1)}g_{n-2}^{q-1}(1,-1) \\ &+2e^{\beta(-\frac{3J}{2}+D_1)}g_{n-2}^{q-1}(0,-1) \\ &+e^{\beta(-3J+2D_1)}g_{n-2}^{q-1}(-1,-1) \\ &+g_{n-2}^{q-1}(0,0) \end{aligned} \quad (7)$$

$$\begin{aligned} g_n(1,1) &= e^{\beta(3J+\frac{9D_2}{2})}g_{n-1}^{q-1}(\frac{3}{2},\frac{3}{2}) \\ &+2e^{(\frac{9\beta D_2}{2})}g_{n-1}^{q-1}(\frac{3}{2},-\frac{3}{2}) \\ &+2e^{\beta(2J+\frac{5D_2}{2})}g_{n-1}^{q-1}(\frac{3}{2},\frac{1}{2}) \\ &+2e^{\beta(J+\frac{5D_2}{2})}g_{n-1}^{q-1}(\frac{3}{2},-\frac{1}{2}) \\ &+e^{\beta(-3J+\frac{9D_2}{2})}g_{n-1}^{q-1}(-\frac{3}{2},-\frac{3}{2}) \\ &+2e^{\beta(-J+\frac{5D_2}{2})}g_{n-1}^{q-1}(-\frac{3}{2},\frac{1}{2}) \\ &+2e^{\beta(-2J+\frac{5D_2}{2})}g_{n-1}^{q-1}(-\frac{3}{2},-\frac{1}{2}) \\ &+e^{\beta(J+\frac{D_2}{2})}g_{n-1}^{q-1}(\frac{1}{2},\frac{1}{2}) \\ &+2e^{(\frac{\beta D_2}{2})}g_{n-1}^{q-1}(\frac{1}{2},-\frac{1}{2}) \\ &+e^{\beta(-J+\frac{D_2}{2})}g_{n-1}^{q-1}(-\frac{1}{2},-\frac{1}{2}) \end{aligned} \quad (8)$$

2.2. Definition of new variables

The number of recursion relations is considerably reduced due to the symmetry of the Cayley tree around the frontier shell. This symmetry induces symmetric relations for g_n and g_{n-1} as follows:

$$g_n(s_0, s_{0'}) = g_n(s_{0'}, s_0) \quad (9)$$
$$g_{n-1}(\sigma_1, \sigma_{1'}) = g_{n-1}(\sigma_{1'}, \sigma_1) \quad (10)$$

New variables $h_n(s_0, s_{0'})$ and $h_{n-1}(\sigma_1, \sigma_{1'})$ are introduced by renormalizing g_n and g_{n-1} by $g_n(0,0)$ and $g_{n-1}(-\frac{1}{2},-\frac{1}{2})$, respectively. In the following we consider:

$$\begin{aligned} X_n &= h_n(1,1) \quad ; \quad Y_n = h_n(1,0) \quad ; \\ Z_n &= h_n(1,-1) \quad ; \quad U_n = h_n(-1,-1) \end{aligned}$$

$$\begin{aligned} w_n &= h_n(0,-1) \quad ; \quad A_{n-1} = h_{n-1}(\frac{3}{2},\frac{3}{2}) \quad ; \\ & B_{n-1} = h_{n-1}(\frac{3}{2},-\frac{3}{2}) \end{aligned}$$

$$\begin{aligned} C_{n-1} &= h_{n-1}(\frac{3}{2},\frac{1}{2}) \quad ; \quad D_{n-1} = h_{n-1}(\frac{3}{2},-\frac{1}{2}) \quad ; \\ E_{n-1} &= h_{n-1}(-\frac{3}{2},-\frac{3}{2}) \quad ; \quad F_{n-1} = h_{n-1}(-\frac{3}{2},\frac{1}{2}) \end{aligned}$$

$$\begin{aligned} G_{n-1} &= h_{n-1}(-\frac{3}{2},-\frac{1}{2}) \quad ; \quad H_{n-1} = h_{n-1}(\frac{1}{2},\frac{1}{2}) \quad ; \\ & I_{n-1} = h_{n-1}(\frac{1}{2},-\frac{1}{2}) \end{aligned}$$

2.3. Expressions of the sublattice magnetizations

By definition, the average value of a physical variable A inside a spin box Λ with specified boundary conditions (b.c) is formally written as:

$$\langle A\rangle_\Lambda^{b.c} = Z_\Lambda^{b.c^{-1}} \sum_{\sigma\in\Omega_\Lambda} Ae^{-\beta H_\Lambda(\sigma/b.c)} \quad (11)$$

where $Z_\Lambda^{b.c}$ is the partition function, σ an element of the space configuration Ω_Λ. Thus, the expressions of the sublattice magnetizations M_A and M_B and the averaged total magnetization per site M are defined respectively by:

$$\begin{aligned} M_A &= \langle s_0\rangle \\ &= \langle s_{0'}\rangle \\ &= Z_A^{-1}\sum_{s_0}\sum_{s_{0'}} s_0 e^{-\beta D_1(s_0^2+s_{0'}^2)}g_n^q(s_0, s_{0'}) \end{aligned} \quad (12)$$

$$
\begin{aligned}
M_B &= \langle \sigma_1 \rangle \\
&= \langle \sigma_{1'} \rangle \\
&= Z_B^{-1} \sum_{\sigma_1} \sum_{\sigma_{1'}} \sigma_1 e^{-\beta D_2(\sigma_1^2+\sigma_{1'}^2)} g_{n-1}^q(\sigma_1, \sigma_{1'})
\end{aligned} \tag{13}
$$

$$
M = \frac{1}{2}(M_A + M_B) \tag{14}
$$

where

$$
Z_A = \sum_{s_0} \sum_{s_{0'}} e^{-\beta D_1(s_0^2+s_{0'}^2)} g_n^q(s_0, s_{0'}) \tag{15}
$$

$$
Z_B = \sum_{\sigma_1} \sum_{\sigma_{1'}} e^{-\beta D_2(\sigma_1^2+\sigma_{1'}^2)} g_{n-1}^q(\sigma_1, \sigma_{1'}) \tag{16}
$$

By setting $M_A = \frac{M_A^{'}}{M_A^0}$ and $M_B = \frac{M_B^{'}}{M_B^0}$ one gets the explicit expressions:

$$
\begin{aligned}
M_A^0 &= e^{(2\beta D_1)}(X_n^q + 2Z_n^q + U_n^q) \\
&\quad +2e^{(\beta D_1)}(Y_n^q + W_n^q) + 1
\end{aligned}
$$

$$
M_A^{'} = e^{(2\beta D_1)}(X_n^q - U_n^q) + e^{(\beta D_1)}(Y_n^q - W_n^q) + 1
$$

$$
\begin{aligned}
M_B^0 &= 2e^{(4\beta D_2)}(A_{n-1}^q + 2B_{n-1}^q + E_{n-1}^q) \\
&\quad +4e^{(2\beta D_2)}(C_{n-1}^q + D_{n-1}^q + F_{n-1}^q + G_{n-1}^q) \\
&\quad +2(H_{n-1}^q + 2I_{n-1}^q + 1)
\end{aligned}
$$

$$
\begin{aligned}
M_B^{'} &= 3e^{(4\beta D_2)}(A_{n-1}^q - E_{n-1}^q) \\
&\quad +4e^{(2\beta D_2)}(C_{n-1}^q - G_{n-1}^q) \\
&\quad +2e^{(2\beta D_2)}(D_{n-1}^q - F_{n-1}^q) + H_{n-1}^q - 1
\end{aligned}
$$

2.4. Formulation of the critical temperatures

By increasing the temperature and keeping fixed all other parameters of the model, SOT temperature can be defined. It is the temperature at which the sublattice magnetizations go continuously and simultaneously to zero without any anomalous behaviour in the Helmoltz free energy F. This so-called Curie Temperature T_c, separates the ferromagnetic order phase from the disordered paramagnatic phase. Some features of the system at T_c may be obtained by setting $M_A^{'}$ and $M_B^{'}$ to zero, i.e., by solving the system of equations: $X_n = U_n$, $Y_n = W_n$, $A_{n-1} = E_{n-1}$, $C_{n-1} = G_{n-1}$, $D_{n-1} = F_{n-1}$ and $H_{n-1} = 1$. By analysing the expressions of the different g_n and g_{n-1} given above, it emerges that at the Curie Temperature T_c, the probability of having a spin up or down may be equal. Technically, we use peaks in the magnetic susceptibility of the system defined by: $\chi \sim (\frac{\partial^2 F}{\partial h^2})_{h=0}$. These new curves simultaneously show a maximum at the same temperature that we take as T_c when no anomalous behaviour is observed in the thermal behaviour of free energy F at this moment. The FOT is obtained when a sharp jump occurs in the thermal behaviours of the sublattice magnetizations followed by a discontinuity of the first derivative of F.

3. Transitions Temperatures and Phase Diagrams

3.1. T=0 phase diagram

Before going into detailed calculations of the phase diagram of the model, we find instructive to first investigate numerically the ground states described by the Hamiltonian (Eqn.1). These states correspond to stable thermodynamic phases. We get four different ground state configurations with different values of $\{M_A, M_B, Q_A, Q_B\}$, namely the ordered ferromagnetic phases $O1 \equiv \left\{1, \frac{3}{2}, 1, \frac{9}{4}\right\}$ or $(\left\{-1, -\frac{3}{2}, 1, \frac{9}{4}\right\})$, $O2 \equiv \left\{1, \frac{1}{2}, 1, \frac{1}{4}\right\}$ or $(\left\{-1, -\frac{1}{2}, 1, \frac{1}{4}\right\})$ and disordered phases $D1 \equiv \left\{0, 0, 0, \frac{9}{4}\right\}$, $D2 \equiv \left\{0, 0, 0, \frac{1}{4}\right\}$, which are indicated in Fig.2 for all q. The disordered phase $D1$ is characterized by the spin configuration where the total value of spin in the sublattice A is zero. This implies $M_A = 0$ because on the sublattice B half of the spins are in $\frac{1}{2}$ state and the other half are in $-\frac{1}{2}$ state, thus leading to $M_B = 0$. The phenomenon is also observed in the disordered phase $D2$. For positive values of Δ_1 and Δ_2, the dominant phase is the ordered phase $O1$. At the points A and B (Fig.2), where the coexistence lines meet, more than two phases coexist.

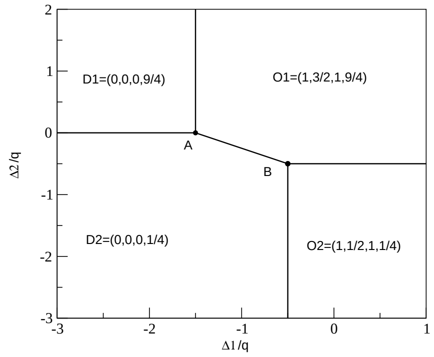

Figure 2: The $T = 0$ phase diagram of the mixed Blume-Capel model (see text) for an arbitrary value of the coordination number q in the (Δ_1, Δ_2) plane. Four stable phases exist, which are denoted by $O1$, $O2$, $D1$ and $D2$, respectively.

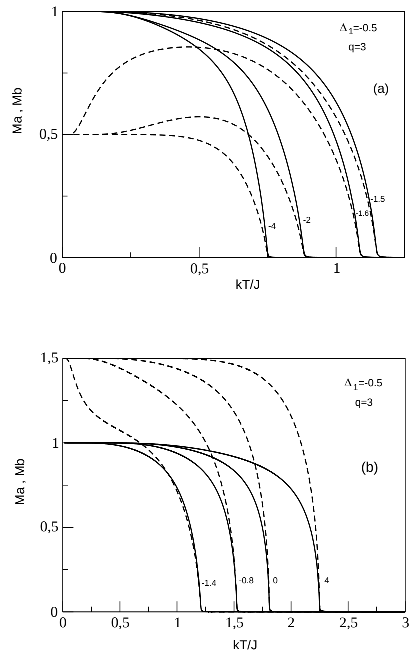

Figure 3: The temperature dependence of the magnetizations M_A and M_B versus kT/J curves when the values of Δ_2 are changed for fixed $\Delta_1 = -0.5$ and $q = 3$.

3.2. Thermal properties of sublattice magnetizations and phase diagrams

In this section, we present the thermal magnetic properties of the magnetizations M_A, M_B and M of the system. In Figs.3 and 4, we have depicted the thermal variation of the sublattice magnetizations M_A and M_B as a function of the temperature for two values of the coordination number q and the reduced crystal-field $\Delta_1 = -0.5$ when the anisotropy field strength of Δ_2 is changed. The results are in perfect agreement with the $T = 0K$ phase diagram concerning the saturation values. Indeed, M_A falls from its unique saturation value 1 to zero with increasing T, whereas M_B shows three saturation values. For both values of q, the curves for M_A and M_B are quite similar to each other and we expect that this should also be true for other values of q. They are all continuous curves of the temperature T, which means that the system exhibits only a second-order transition for the selected values of Δ_2. When going from $q = 3$ to $q = 4$, the temperature T_c at which the transition to the disordered phase (with zero net magnetization) occurs moves to higher temperature values when Δ_2 increases, whereas with decreasing values of Δ_2, the opposite holds.

As shown in Fig.3 (q=3), for $\Delta_2 \geq -0.8$, the sublattice magnetization M_B has a standard characteristic convex shape. When Δ_2 decreases from -0.8 however, the temperature dependence of M_B may exhibit a rather rapid decrease from its saturation value at $T = 0K$. The phenomenon is further increased when the value of Δ_2 approaches the boundary between the $O1$ phase and the $O2$ phase ($\Delta_2 = -1.5$). Particularly, for $\Delta_2 = -1.5$ the saturation value of M_B is equal to 1, which implies that the first half of spins on the sublattice B are equal to $\frac{3}{2}$(or $-\frac{3}{2}$) and the second half are equal to $\frac{1}{2}$(or $-\frac{1}{2}$). In our case ($J > 0$), the averaged magnetization M is equal to 1. As the value of Δ_2 is further decreased, the ground state becomes $O2$ with M_B equal to 0.5 at $T = 0K$. For $\Delta_2 < -1.5$, the thermal variation of M_B exhibits different behavior depending on the values of Δ_2. Precisely, for $-4 < \Delta_2 < -1.5$, an interesting feature is the initial rise of M_B with an increase in temperature and then decreasing to zero. This behavior of M_A and M_B are similar for $q = 4$ (Fig.4), but here, the boundary value of Δ_2 is equal to -2. This result is in agreement with Fig.2 of [18] and Fig.3 of [25] also with our phase diagram at $T = 0K$.

Fig.5 shows the temperature dependencies of the total averaged magnetization M when $\Delta_1 = -0.5$ with various values of Δ_2. The total magnetization

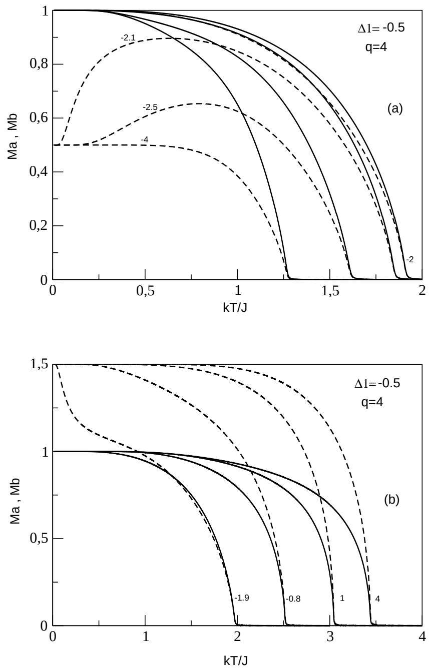

Figure 4: The temperature dependence of the magnetizations M_A and M_B versus kT/J curves when the values of Δ_2 are changed for fixed $\Delta_1 = -0.5$ and $q = 4$.

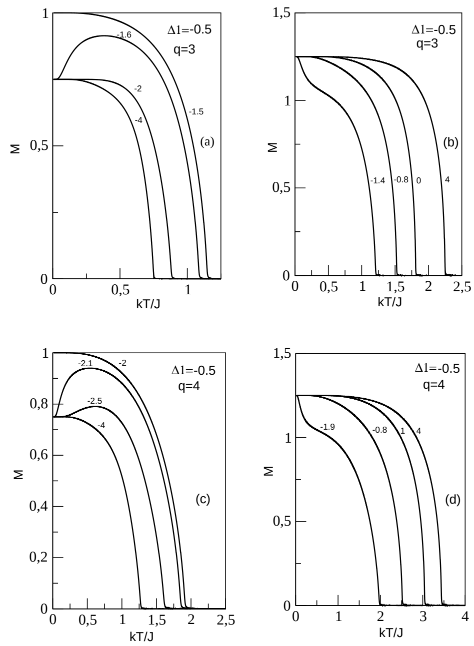

Figure 5: The temperature dependence of the total magnetization M versus kT/J curves when the values of Δ_2 are changed for fixed $\Delta_1 = -0.5$ for $q = 3$ and $q = 4$.

M presents similar behavior like M_A and M_B. M shows three saturation values at $T = 0K$: 0.75, 1 and 1.25. This result is in agreement with Fig.2 of [18].

Here, we examine the phase diagrams of the mixed spin-1 and spin-3/2 ferromagnetic Blume-capel Ising model on the two-fold Cayley tree. In Figs.6 and 7, the solid lines are used for second-order transition while the dashed line, denoted by Lt, represents the positions of the tricritical points and the full circle represents the tricritical end-points.

First, we consider the case where $\Delta_1 = \Delta_2 = \Delta$ and we obtain the resulting phase diagram in $(\Delta, kT/J)$ plane for $q = 3, 4$ and 6. From Fig.6, we note that: for all values of the coordination number q the system exhibits a tricritical point. The second-order line starts from this tricritical point and increases with the increasing values of Δ. This result is in perfect agreement with Fig.7 of [23]. The temperature of the tricritical points increases with the coordination number q. It is important to mention that the tricritical points appear at large negative values of Δ for all values of q.

Second, we obtain the resulting phase diagrams in $(\Delta_1, kT/J)$ plane for different values of Δ_2 when $q = 3, 4$. The critical lines are labelled with values of Δ_2. It is noted from Fig.7, that the phase diagrams are topologically similar. In Fig.7, three phases are shown: P is used for paramagnetic phase and $O1$ and $O2$ denoted the two ordered ferromagnetic phases. We show in Fig.7(a) the phase diagram of the model at fixed values of Δ_2 and varying value of Δ_1 for $q = 3$. From this figure, one can clearly observe that for $-4, 5 < \Delta_1 < -1.5$, the tricritical behaviour appears. In this domain, the tricritical line Lt presents two end-points: $A1$ and $B1$. From a different perspective, Fig.7(b) shows the phase diagram of the model for $q = 4$. We notice that the tricritical behaviour exists in the region $-6 < \Delta_1 < -2$. In this region, the Lt presents again two end-points: $A2$ and $B2$. These results obtained are in agreement Fig.3(a,b) of [22] and Fig.2(a) of [25]. It is important to mention that the width of the tricritical domain increases with the coordination number q.

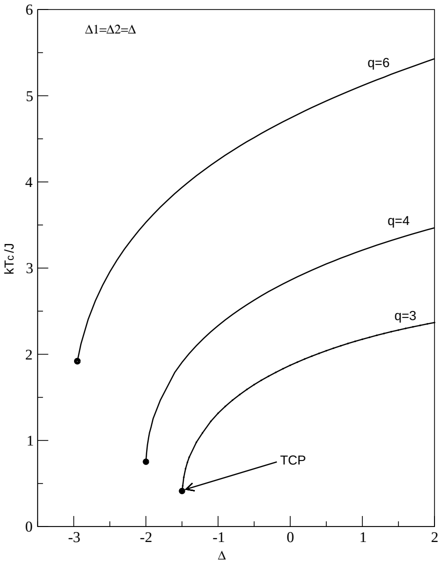

Figure 6: Finite temperature phase diagrams of the model in the $(\Delta, kTc/J)$ plane for $q = 3, 4$ and 6. The tricritical (TCP) is indicated by the full circle.

4. Conclusion

In summary, the magnetic properties of the mixed spin-1 and spin-3/2 Blume-Capel on the two-fold Cayley tree are studied using the exact recursion relations method (Fig.1). The resulting phase diagrams of this model are presented for the coordination numbers $q = 3, 4$ and 6. First, we have studied the thermal properties of the magnetization of each sublattice and the net magnetization. The result is compared to those obtained by Z. H. Xin et al., who used the effective-field theory with correlation to study the same model [18]. Good agreement was also noticed with the $T = 0$ phase diagram (Fig.2). Second, we have found that when the strengths of the crystal-field of the sublattices are equal, the system exhibits a tricritical point (TCP) for all values of the coordination number q. This result is in perfect agreement with those obtained by C. Ekiz who used the same method to study the mixed spin-1 and spin-3/2 on the Bethe lattice in ferromagnetic version [23]. Finally, we studied the resulting phase diagrams of the model in $(\Delta_1, kT_c/J)$ plane when the crystal field strengths are not equal; the system presents interesting properties.

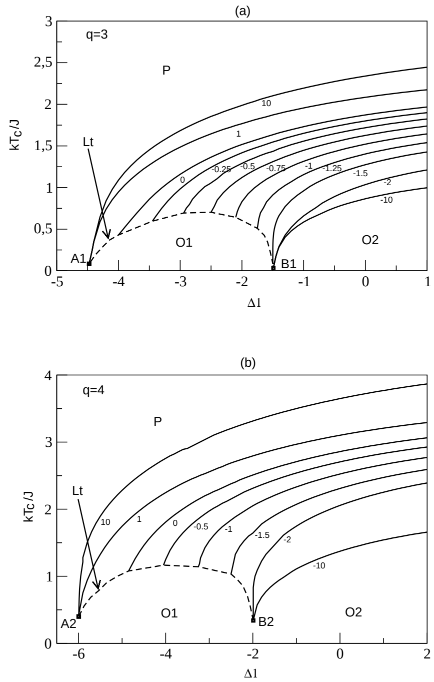

Figure 7: The critical temperature of the model as a function of the crystal-field interaction Δ_1 for $q = 3$ and $q = 4$. The number accompanying each curve denotes the values of the crystal-field interaction Δ_2. Lt indicates the tricritical line. $A1$ and $B1$ indicated by the full square are the end-points of Lt line for $q = 3$. $A2$ and $B2$ indicated by the full square are the end-points of Lt line for $q = 4$.

Acknowledgments

This work is partially supported by the Abdus Salam International Centre for Theoretical Physics (ICTP), Trieste, Italy.

References

[1] O. Khan, *Molecular Magnetism* (VCH, New York, 1993).

[2] M. Monsuripur, J. Appl. Phys. **61**, 1580 (1987).

[3] N. Benayad and J. Zittartz, Z. Phys. B. Condensed

Matter **81**, 107 (1990);
S. L. Schofield and R. G. Bowers, J. Phys. A: Math. Gen. **13**, 3697 (1980).

[4] B. Y. Yousif and R. G. Bower, J. Phys. A: Math. Gen. **17**, 3389 (1984).

[5] F. K. Tang, J. Phys. A: Math. Gen. **21**, L1097 (1988).

[6] C. Ekiz, Physics Lett. A **352**, 291 (2006).

[7] T. Iwashia and N. Uryu, Phys. Lett. A **96**, 311 (1983);
T. Iwashia and N. Uryu, J. Phys. Soc. Jpn. **53**, 721 (1984);
T. Iwashia and N. Uryu, Phys. Stat. Sol. (b) **125**, 551 (1984).

[8] T. Kaneyoshi, Phys. Rev. B **34**, 7866 (1986);
T. Kaneyoshi, J. Phys. Soc. Jpn. **56**, 2675 (1987);
T. Kaneyoshi, ibid. **58**, 1755 (1989);
T. Kaneyoshi, J. Magn. Magn. Mater. **98**, 201 (2000).

[9] T. Kaneyoshi, Solid State Commun. **70**, 975 (1989).

[10] T. Kaneyoshi, E. F. Sarmento and I. F. Fittipaldi, Phys. Stat. Sol. (b) **150**, 261 (1988);
J. A. Plascak, Physica (A) **198**, 655 (1993).

[11] T. Kaneyoshi and J. C. Chen, J. Magn. Magn. Mater. **98**, 201 (1991).

[12] N. Benayad, A. Klumper, J. Zittartz and A. Benyoussef, Z. Phys. B: Condensed Matter **77**, 333 (1989).

[13] G. M. Zhang and C. Z. Yang, Phys. Rev. B **48**, 9452 (1993).

[14] G. M. Buendia and M. A. Novotny, J. Phys. Condensed Matter **9**, 5951 (1997).

[15] H. F. V. De Resende, F. C. Sa Barreto and J. A. Plascak, Physica A **149**, 606 (1988).

[16] J. W. Tucker, J. Magn. Magn. Mater. **195**, 733 (1999).

[17] A. Bobák, Phys. Stat. Sol. (b) **150**, 261 (1988).

[18] Z. H. Xin, G. Z. Wei and T. S. Liu, J. Magn. Magn. Mater. **188**, 65 (1998);
Z. H. Xin, G. Z. Wei and J. Wei, J. Magn. Magn. Mater. **204**, 144 (1999);
A. Bobák, Physica (A) **258**, 140 (1998);
Z. H. Xin, G. Z. Wei and J. Wei, Physica (A) **293**, 455 (2001).

[19] Z. H. Xin, G. Z. Wei and T. S. Liu, J. Magn. Magn. Mater. **188**, 65 (1998).

[20] A. Bobák, O. F. Abubrig and D. Horváth, J. Magn. Magn. Mater, in press.

[21] A. Bobák, O. F. Abubrig, D. Horváth and M. Jascur, Physica (A) **296**, 437 (2001).

[22] E. Albayrak, Int. J. Mod. Phys. B, **17**, 1087 (2003).

[23] C. Ekiz, J. Magn. Magn. Mater. **307**, 139 (2006).

[24] R. A. Yessoufou, S. H. Amoussa and F. Hontinfinde, Cent. Eur. J. Phys. **7**, 555 (2009).

[25] A. Bobák, O. F. Abubrig and D. Horváth, J. Magn. Magn. Mater. **246**, 177 (2002).

Received: 30 March, 2011
Accepted: 23 August, 2011